Nanotopography induced contact guidance of the F11 cell line during neuronal differentiation: a neuronal model cell line for tissue scaffold development

2012 Nanotechnology 23 275102

(http://iopscience.iop.org/0957-4484/23/27/275102)

Nanotechnology **23** (2012) 275102 (14pp) doi:10.1088/0957-4484/23/27/275102

Nanotopography induced contact guidance of the F11 cell line during neuronal differentiation: a neuronal model cell line for tissue scaffold development

Paul Wieringa[1,2,3], **Ilaria Tonazzini**[4], **Silvestro Micera**[1,5] **and Marco Cecchini**[4]

[1] The BioRobotics Institute, Scuola Superiore Sant' Anna, Viale le Rinaldo Piaggio 34, 56025 Pontedera, Italy
[2] Center for Micro-BioRobotics, Italian Institute of Technology (IIT), Viale le Rinaldo Piaggio 34, 56025 Pontedera, Italy
[3] MIRA Institute for Biomedical Technology and Technical Medicine, Department of Tissue Regeneration, University of Twente, P.O. Box 217, 7500 AE, Enschede, The Netherlands
[4] National Enterprise for nanoScience and nanoTechnology (NEST), Scuola Normale Superiore and Istituto Nanoscienze-CNR Piazza San Silvestro 12 56127 Pisa, Italy
[5] Translational Neural Engineering Laboratory, Center for Neuroprosthetics & Institute of Bioengineering (IBI)—School of Engineering, École Polytechnique Fédérale de Lausanne (EPFL), BM 3114 (Bâtiment BM), Station 17, CH-1015 Lausanne, Switzerland

E-mail: paul.wieringa@sssup.it

Received 12 February 2012, in final form 8 May 2012
Published 19 June 2012
Online at stacks.iop.org/Nano/23/275102

Abstract
The F11 hybridoma, a dorsal root ganglion-derived cell line, was used to investigate the response of nociceptive sensory neurons to nanotopographical guidance cues. This established this cell line as a model of peripheral sensory neuron growth for tissue scaffold design. Cells were seeded on substrates of cyclic olefin copolymer (COC) films imprinted via nanoimprint lithography (NIL) with a grating pattern of nano-scale grooves and ridges. Different ridge widths were employed to alter the focal adhesion formation, thereby changing the cell/substrate interaction. Differentiation was stimulated with forskolin in culture medium consisting of either 1 or 10% fetal bovine serum (FBS). Per medium condition, similar neurite alignment was achieved over the four day period, with the 1% serum condition exhibiting longer, more aligned neurites. Immunostaining for focal adhesions found the 1% FBS condition to also have fewer, less developed focal adhesions. The robust response of the F11 to guidance cues further builds on the utility of this cell line as a sensory neuron model, representing a useful tool to explore the design of regenerative guidance tissue scaffolds.

S Online supplementary data available from stacks.iop.org/Nano/23/275102/mmedia

(Some figures may appear in colour only in the online journal)

1. Introduction

This work introduces the F11 neuronal cell line as a suitable tool for the development of tissue scaffolds specific for the regeneration of the peripheral nervous system (PNS). The response of neurite growth to nanotopographical guidance cues is analyzed, towards a more effective scaffold design.

Over the past few decades, many studies have investigated the use of engineered synthetic tissue scaffolds for *in vivo* neural tissue repair and regeneration. These examples, though functional, often perform poorly with respect to the 'golden standard' of the autograph [1–3]. Thus far, scaffold design has relied on intuition and accumulated knowledge, which has led to increasingly complex, multicomponent scaffolds which incorporate structural guidance cues, chemical cues, and supporting glial cells [4–8]. While these works show great improvements, the trial-and-error approach that is still employed intrinsically limits neural repair to what is achievable instead of what is desired.

The production of effective and efficient tissue engineered systems requires an intelligent design approach for tissue scaffolds, with reliance on tools and methods to further understand and manipulate the biological systems in question. As neural regenerative investigations continue, a complex picture is emerging of neural pathfinding and cellular response to the extracellular components within the body, including growth factors [9], ligand-binding extracellular matrix (ECM) proteins [10], and the mechanical properties of the ECM [11].

Particularly relevant to scaffold design is the role of mechanical cues and their effect on cellular differentiation, migration and guidance. Cascades of intracellular signals which dictate cell behavior can be influenced by the surface properties of the materials employed, the presence of extracellular proteins and peptides, nanotopographical structures, and even the mechanical properties of the underlying scaffold [12–17]. While this provides a wealth of possibilities for attaining highly functional tissue scaffolds, it also presents a great challenge to understand which extracellular signals are relevant and how to best implement them.

In particular, the influence of micro- and nanotopography on neurite outgrowth has been explored under various conditions, both *in vitro* [18, 19] and *in vivo* [20, 21]. Many neuronal cell types have been investigated, including primary central nervous system (CNS) neurons, PNS neurons and neuronal secondary cell lines. The ability to direct neurite growth has been shown to depend on both the dimensions of the underlying patterned substrate and, importantly, the cell type [22–25]. In particular, the work of Raijnek *et al* [23] highlights the importance of using a representative neuronal model: *xenopus* spinal neurons are shown to grow parallel to microstructure compared to rat hippocampal neurons, which grow perpendicular.

Cells explore their surroundings by extending filopodia and lamellipodia from the lamella at the cell periphery, probing the surrounding environment. Mechanical cell guidance is mediated via the mechanisms of cell adhesion, notably the formation and maturation of focal adhesion (FA) complexes. The reader is directed to recent reviews on this subject by Geiger *et al* [26] and Scales *et al* [27]. Initial cell adhesion begins with integrin transmembrane receptors binding to extracellular proteins, forming nascent FAs and an initial linkage to actin fibers of the cytoskeleton. The actin fibers apply force to integrins and those that resist coalesce to form FA complexes and, later, mature FAs. FAs which do not provide sufficient adhesion are disassembled.

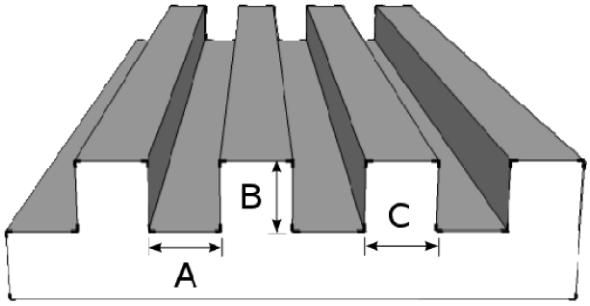

Figure 1. The dimensions of the nanograting patterned culturing substrate. A groove width of 500 nm (A) and groove depth of 300 nm (B) was used for all experiments. Different ridge widths (C) were employed to investigate the role of restricting focal adhesion formation on neurite guidance.

New protrusions then extend from regions with successful FA formation, biasing the net direction of cell motion in that direction. Therefore, the ability to influence focal adhesion formation allows control of cell shape and guidance of neurite outgrowth.

Previous findings from our group have confirmed an association between the development of focal adhesions, the underlying nanograting patterned substrate, and the resulting PC12 cell polarity and neurite outgrowth direction [24, 28]. The grating is a repeating ridge–groove nanopattern such that focal adhesion formation is restricted and, depending on the ridge dimension, the FA can only expand in the direction of ridge orientation. This induced polarization imparts direction upon the cell, establishing a physiological basis for the observed influence of topographical guidance cues.

In applying this examination to the case of peripheral neuron regeneration, this paper represents the first time the F11 cell line has been used to study cell response to nanopatterned substrates. The F11 cell line is a hybridoma of a rat dorsal root ganglion (DRG) cell and a mouse neuroblastoma [29]. In contrast to a typical heterogeneous DRG population comprised of different sensory neuron subtypes, the F11 cell line represents a homogeneous population, exhibiting markers and receptors of nociceptive sensory neuron lineage [30, 31] and producing an electrical response to nociceptive stimuli [32, 33]. Previously used as a model for differentiation [34], cytoskeletal reorganization and plasticity [35], and for studies of gene regulation during PNS regeneration [36], this work establishes the F11 as a functional DRG model for providing insight into mechanical guidance during nerve regeneration.

The response of F11 cells to nanograting patterns of various dimensions (see figure 1) and under different medium compositions is explored. We highlight the biomolecular response in terms of cytoskeletal organization and focal adhesion formation, capitalizing on the utility of this cell line to assess the influence of nanotopographical cues towards an improved tissue scaffold for the peripheral nervous system.

2. Materials and methods

2.1. Cell culturing

F11 hybridoma cells (a kind gift from Dr Ratto, CNR, Pisa, Italy) are a fusion of a mouse dorsal root ganglion and a rat neuroblastoma. They were grown in Dulbecco's Modified Eagle Medium (DMEM) with the addition of 10% fetal bovine serum (FBS), penicillin (10 units ml^{-1}), streptomycin (10 mg ml^{-1}) and l-glutamine (2 mM) [33] in an incubator at 37 °C and 5% CO_2. The cells were grown in standard tissue-culture treated dishes and the medium was refreshed every 2 days until the cell growth was confluent (approximately every 4 days), at which point the cells were dissociated using EDTA–trypsin (0.05%) and passaged 1:15. The experiments used cells from passages 10–14. All culturing materials were purchased from Invitrogen unless otherwise stated.

2.2. Substrate manufacturing

The substrate material used was cyclic olefin copolymer (COC) from Ibidi, a thermoplastic polymer with excellent optical properties subjected to a proprietary tissue-culture treatment to enhance cell adhesion. Nanotopography was introduced to the substrates via nanoimprint lithography (NIL), as described previously [24].

Briefly, imprinting molds were fabricated by spin coating a thin film of PMMA onto a p-doped silicon wafer. Electron beam lithography was used to create a negative mask of the nanopattern grating in the PMMA layer and subsequent RIE etching was performed. The remaining PMMA was removed to reveal the relief nanopattern of grooves and ridges, with an approximate groove depth of 350 nm. Six different nanograting patterns were investigated, each maintaining a constant groove width of 500 nm but with different ridge widths of 500, 750, 1000, 1250, 1500, or 2000 nm. The patterns covered an area of 16 mm^2. The pattern substrates were glued to Wilco dishes using silicone glue (RS692-524, RS Components). As a control, flat COC culture dishes were used (μ-Dish$^{35\ mm,\ low}$, Ibidi). The dishes were sterilized with ethanol and rinsed twice with sterile PBS before cell seeding.

2.3. Cell seeding and differentiation

The cells were trypsinized, resuspended in culture medium and seeded on substrates with a density of approximately 6000 cells cm^{-2}. The cell suspension was left for 3 h at 37 °C and 5% CO_2, to allow the cells to attach. The medium was then removed and replaced with differentiation medium consisting of DMEM, penicillin (10 units ml^{-1}), streptomycin (10 mg ml^{-1}), l-glutamine (2 mM), and forskolin (10 mM) (FSK) to stimulate differentiation. Two different serum concentrations were investigated: 1% FBS concentration, reflecting the established differentiation protocol for this cell line [34], and the standard growth medium concentration of 10% FBS, mimicking the conditions of our previous work with PC12 cells [24]. The substrates were used first for the 10% FBS experiment, then cleaned with EDTA–trypsin for 30 min at 37 °C and 5% CO_2 followed by a 3× PBS wash. The substrates were then used for the 1% FBS experiment. The cells were maintained at 37 °C and 5% CO_2 and the differentiation medium was refreshed every 2 days.

2.4. Data acquisition

The cell cultures were examined for cell body growth and neurite elongation 24, 48, 72 and 96 h after FSK stimulation. 8 bit gray scale images were recorded with a Nikon TI using a DIC and a 40× oil-immersion objective or a 20× objective, depending on the extent of neurite growth. Images for cell counting were acquired using a 10× objective, an epifluorescent source and a DAPI filter cube. Images were processed and measurements performed with the Fiji/Imagej image processing software and associated plugins. Each experimental condition was repeated three times.

2.4.1. Cell morphology measurements. Cell bodies were quantified using the LiveWire ImageJ plugin, developed by Daniel Lelis Baggio. Only cells that were distinguishable and exhibited measurable neurite outgrowth, as specified above, were considered. When possible, a minimum of 30 cell bodies was recorded per substrate, per day.

In addition to cell body area, the average cell body diameter was also found only for day 1, flat substrates, both medium conditions. This length has been traditionally used as the neurite length threshold, such that the analysis only considered 'mature' neurites [37]. The average value (approximately 35 micrometers, in line with [38]) was used as a threshold for later neurite analysis.

Image sequences of neurites longer than a single image frame were merged into a single image with a 2D stitching plugin (developed by Stephan Preibisch). Neurite extensions were traced with the NeuronJ plugin (developed by Erik Meijerink) from the point of origin at the perimeter of the cell body to the tip of the neurite growth cone. At bifurcation points of neurites, a single neurite path was traced by selecting the thicker, longer branch of the extension (in that order). Only neurites which terminated in a free end or with growth cones cleanly abutting neighboring cells were considered. Neurites whose growth was obstructed or altered by other neurites or cell bodies were disregarded. A minimum of 40 individual neurons was recorded per substrate, per day.

Neurite length was measured in terms of actual length (the distance of the traced neurite path) and only neurites above the length threshold, described above, were included. Also investigated was the number of neurites per cell, examining whether nanogratings increase the incidence of uni/bipolar neurons versus neurons with three or more neurite extensions.

2.4.2. Contact guidance measurements. The Feret (or caliper) angle of the cell was used to describe the alignment of the cell body with respect to the underlying substrate orientation. To measure the influence of patterned substrates on cell body morphology, the cell circularity was calculated (equal to $4 * \pi$ (area/perimeter^2)) as a number between 0 and

1 to indicate the degree of elongation of the cell body (lower values indicate more elongation).

Neurite alignment was measured by approximating the neurite as a straight line from the initiation point to the end point and taking the relative angle of this line with respect to the underlying nanograting orientation.

For all measurements, the orientation of the grating was found by using a subsection of a reference image that was free of cells (with only the nanopatterned surface). The angle was extracted using the Fourier Component Analysis of the Directionality plugin (by Jean Yves Tinevez). Flat substrates were given a 0 grating angle.

2.4.3. Cell proliferation assay. Flat substrates and patterns with 500 nm ridges and 2000 nm ridges were examined, representing the extremes of the patterns used. The substrates were produced as before, then punched out into 6 mm diameter discs to fit inside a 96 well plate (Nunc). Viton® polymer rings (Eriks b.v., The Netherlands), with an outer diameter of 6.5 mm and inner diameter of 5 mm, were sterilized in 70% ethanol and inserted into the wells to hold the substrates to the bottom. They also served to confine seeded cells to patterned substrate only. The wells were sterilized with ethanol, washed three times with PBS, then filled with growth medium containing 10% FBS (200 ml per well). The substrates were seeded at 7500 cells cm^{-2} (minimum cell requirement for metabolic assay), in triplicate, and both the 10% and 1% serum conditions were investigated as before. The cells were cultured over a four day period, with a medium change on day 2.

As a measure of metabolic activity, PrestoBlue (Invitrogen) assays were performed on days 2 and 4, coinciding with medium changes. The medium was replaced with identical medium containing 10% PrestoBlue solution, 300 ml per well. Three blank wells were also filled for reference. The substrates were incubated at 37 °C and 5% CO_2 for 2 h in the dark.

100 ml was transferred from the sample wells to a white, solid-bottom 96 well plate (Nunc) and the fluorescence was measured, correlating to cell metabolic activity, using a Perkin Elmer Victor^3 1420 multilabel counter (top-read; excitation filter: 560/10; emission filter: 590/10). A duplicate measure of the resulting solution was performed and averaged and corrected for background fluorescence. The average and standard deviations were calculated from the experimental triplicates. Per day and serum concentration, a one-way ANOVA test was used to compare substrates. A paired T test was used to compare the same conditions at days 2 and 4.

On day 4, Hoechst 33 342 (Invitrogen) nuclei stain was applied and the cells were counted to determine the final number of cells. The substrates were washed one time with PBS after the PrestoBlue assay, followed by 200 ml of medium containing 2 mg ml^{-1} Hoechst solution. This was left to incubate for 25 min at 37 °C and 5% CO_2, after which the substrates were washed once with PBS and replaced with PBS for imaging. Using a 10× objective, five non-overlapping images were collected. Per sample, the average number of cells per cm^2 was calculated. The average and standard deviations were calculated from the experimental triplicates. Per serum concentration, a one-way ANOVA test was used to compare substrates. A *T* test was used to compare identical substrates with different serum concentrations.

2.4.4. Immunocytochemistry—nucleus, actin and focal adhesion staining. For fluorescence immunocytochemistry, F11 cells, FSK-stimulated on different nanogratings (flat COC, 1 and 2.5) for 24 h or 96 h, were processed as previously reported [35]. Briefly, the cells were fixed for 15 min in 4% paraformaldehyde with 4% sucrose in PBS at room temperature, washed in PBS and then incubated with the primary antibody anti-vinculin (Sigma; mouse, monoclonal, dil. 1:100) and phalloidin Alexa Fluor 647 (Invitrogen; 1:20) in GDB buffer (0.2% gelatin, 0.8 M NaCl, 0.5% Triton X-100, 30 mM phosphate buffer, pH 7.4), overnight at 4 °C.

The samples were then washed and incubated with secondary antibody conjugated to Alexa Fluor 488 (Invitrogen; anti-mouse, dil. 1:100) in GDB buffer, for 2 h at room temperature. The samples were washed twice and mounted with Vectashield mounting media (Vector Labs) containing DAPI (to visualize the cell nuclei). The fluorescent samples were then examined with a Leica SP2 confocal microscope. Negative control experiments were also performed, replacing the incubation with the primary antibody with a blocking solution; the staining was absent on these samples.

2.5. Statistical analysis

For each metric considered, comparisons between each condition were usually made by averaging the mean values of each condition (repeated in triplicate). The exception was the number of neurites per cell, which used the average of the medians for further analysis. The means of each repeated experiment were assumed to be normally distributed about the true mean, with normality confirmed via a Shapiro–Wilks test (alpha = 0.01) available within the R statistical software. Data are shown with the standard error of the mean (mean ± SEM, $n = 3$).

For analysis between conditions over the four day period, a repeated measured (mixed-model) ANOVA analysis was performed. When comparing different culture medium and substrates at a single time point, a regular two-way ANOVA analysis was used. When examining growth at a single time point for one culturing medium (1% or 10% FBS), a one-way ANOVA analysis was performed. Where applicable, all analysis was followed by a *post hoc* Bonferroni test to further specify differences. A significance level of 0.05 was used, unless otherwise stated. This statistical analysis was performed using the Graphpad Prism software package (GraphPad Software, San Diego, CA, USA) and R statistical software in combination with the Deducer package (www.r-project.org/).

3. Results

3.1. Qualitative assessment

Observations of F11 cell growth showed that the cell bodies and neurites were generally well aligned on all the patterned substrates compared to the flat control condition (figure 2).

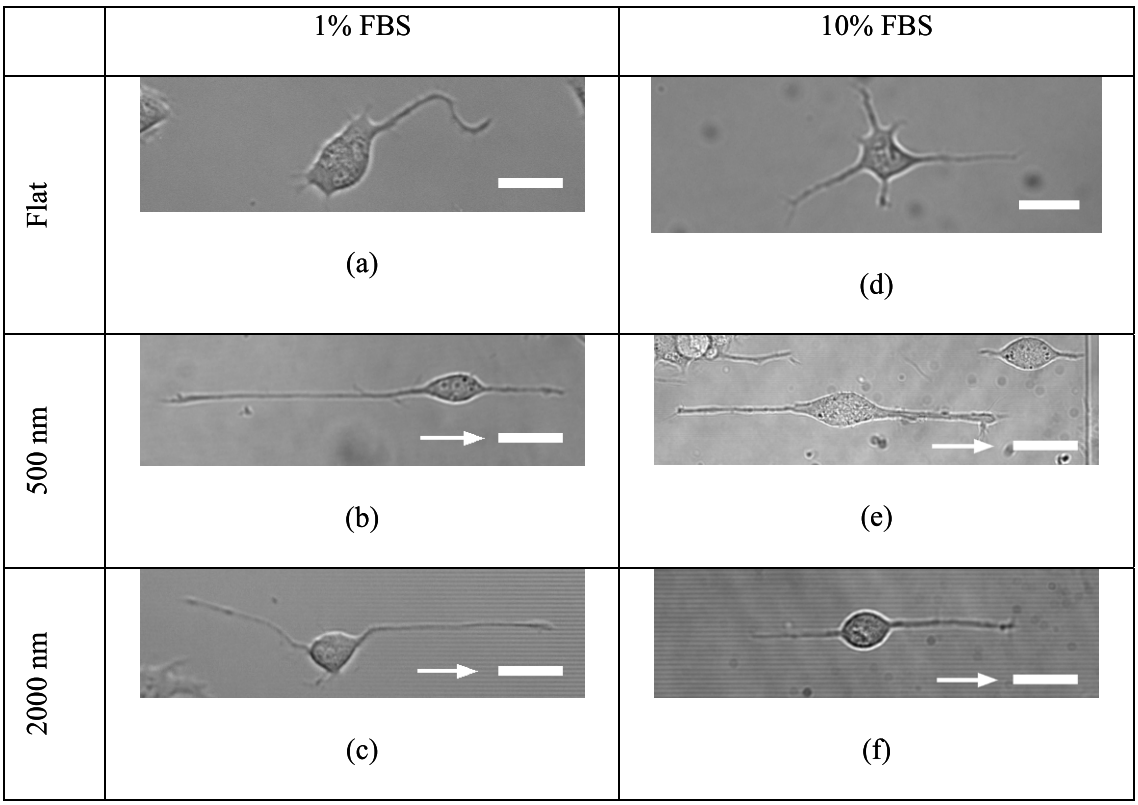

Figure 2. F11 hybridoma cultured on various substrates on day 1. Flat substrates (a), (d) exhibit notably less cell polarization compared to both the 500 nm ridge patterns (b), (e) and the 2000 nm ridge patterns (c), (f). Images (a)–(c) show cells grown in 1% FBS, while (d)–(f) show cells grown in 10% FBS. The arrow indicates the direction of the grating pattern; the scale bar indicates 35 mm.

The 1% FBS condition permitted differentiation and extensive neurite outgrowth while limiting cell division. Sufficient cell–cell contact appeared to be required for survival; a seeding density below 5000 cells cm^{-2} led to poor cell viability. The 10% FBS condition was performed for comparison to the culture conditions of the previous PC12 experiments, as well as to improve the cell viability in low density cultures. However, the 10% FBS condition experienced extensive cell division, reaching confluence and resulting in difficulty in achieving consistent measurements of non-occluded neurites and cells over the four day period.

3.2. Cell morphology

Morphometric measurements of the cell body area revealed a notable change in cell body area over time between different culture media: 1% FBS had a general increase while the measurable cells of the 10% FBS condition first increased and then decreased. However, per culture medium at identical time points, no significant difference in cell area was observed with respect to different culturing substrates (including the flat control, figure 3).

Both the 1% and 10% FBS conditions exhibit no significant difference in cell circularity on any substrate over the four day period, with an overall average of 0.75 (see supplementary data, tables 1 and 2 available at stacks.iop.org/Nano/23/275102/mmedia).

Examining the length of neurite outgrowth shown in figure 4, one sees that there is no difference between substrate conditions for either the flat or the patterned surface condition. However, there is a distinct increase in length over time, as expected. Comparing the day 4 neurite lengths, the 1% FBS neurites are distinctly longer compared to the 10% FBS neurites ($p < 0.0001$, two-way ANOVA).

Examining the number of neurites per cell, we find that in the 1% FBS condition a more prevalent bipolar morphology is established (figure 5). In comparison, the 10% FBS condition shows no temporal trend: for each time point, there is no difference between substrates (patterned or the flat control) for either culture condition.

3.3. Contact guidance

Examining the alignment of the actual cell body to the underlying nanopattern (see figure 6), the 1% FBS shows a distinct difference between the patterned conditions and the flat control condition, at all time points. The 10% FBS condition shows a variable pattern of significant differences between the patterned and the flat control conditions. However, no significant differences between patterned substrates were observed for both culture conditions.

Analysis also shows that there is a significant change ($p < 0.05$) over time for the 10% and 1% FBS conditions as the cell bodies become less aligned.

Similarly to the cell bodies, a two-way mixed-model ANOVA analysis of neurite alignment shows that the nanopatterned substrates induce neurite alignment to their

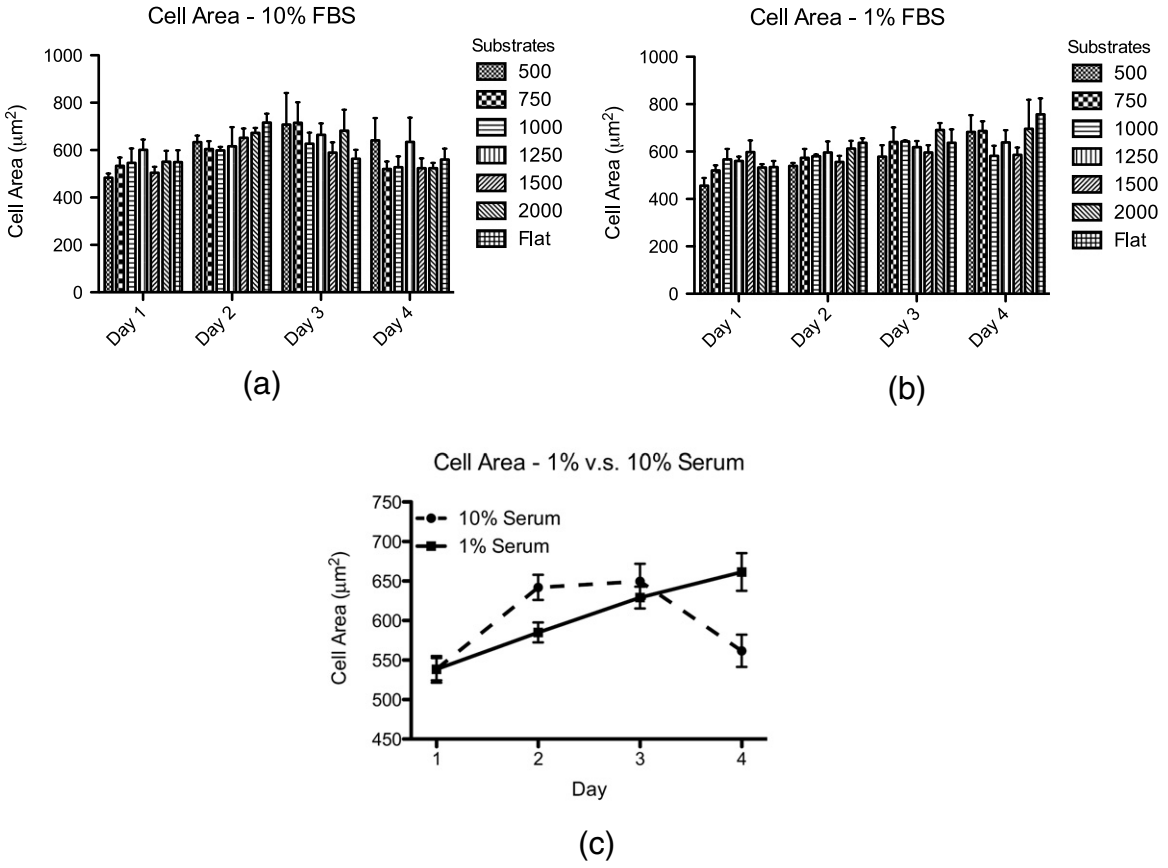

Figure 3. Cell body area measurements on different substrate patterns over a four day period for (a) 10% and (b) 1% FBS. A comparison (c) of the average cell area (all substrate conditions combined) over the four day period shows a significant change over the four day period ($p < 0.0001$) for both culturing conditions. (Mean ± SEM, $n = 3$, >8000 cells measured.)

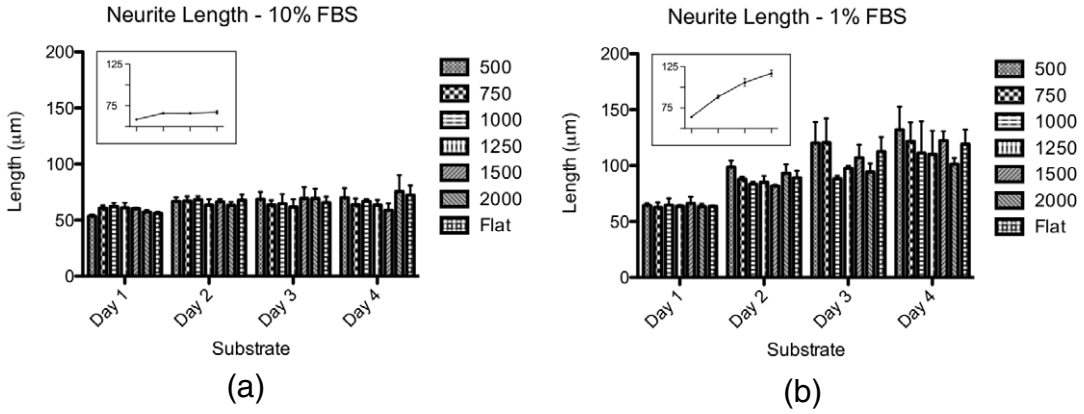

Figure 4. The average neurite length over a four day period on different substrates and with different culturing conditions: (a) 10% FBS; (b) 1% FBS. No differences between conditions were noted within the same time point, though statistically significant differences over time were detected ($p < 0.05$ for 10% FBS; $p < 0.0001$ for 1% FBS). The inset shows the average neurite length over all conditions for the four day period. By day 4, the neurites are longer under the 1% serum compared to the 10% serum ($P < 0.0001$). (Mean ± SEM, $n = 3$, >15 000 neurites analyzed.)

topographical signal, compared to the control flat substrate in both culture conditions (figures 7(a)–(b)).

Examining only the patterned substrates (flat controls not included), a trend can be observed of decreasing neurite alignment with increasing ridge width and in particular for the 10% FBS condition. Since a mixed-model ANOVA analysis (per serum condition, all groups over the four day period) found no significant differences between patterned substrates for both the 1% and 10% FBS conditions, a one-way ANOVA analysis was applied to single time points (per serum condition, all groups on individual days) in order to increase the statistical power. This confirmed the observable trend for

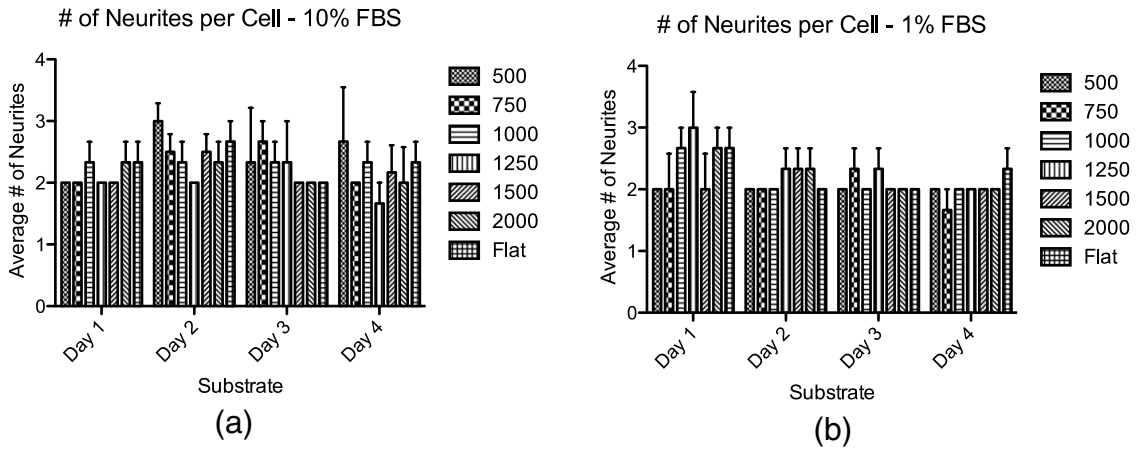

Figure 5. The average median of neurites per cell for both the (a) 10% FBS and (b) 1% FBS culturing conditions over a four day period on different substrates. Per time point, no significant difference is found between different substrates, the 1% FBS condition is found to have a significant decrease in the number of neurites per cell over time ($p < 0.01$, two-way ANOVA), with an emerging prevalence of bipolarity (mean $\pm$ SEM, $n = 3$, >7000 total number of cells analyzed).

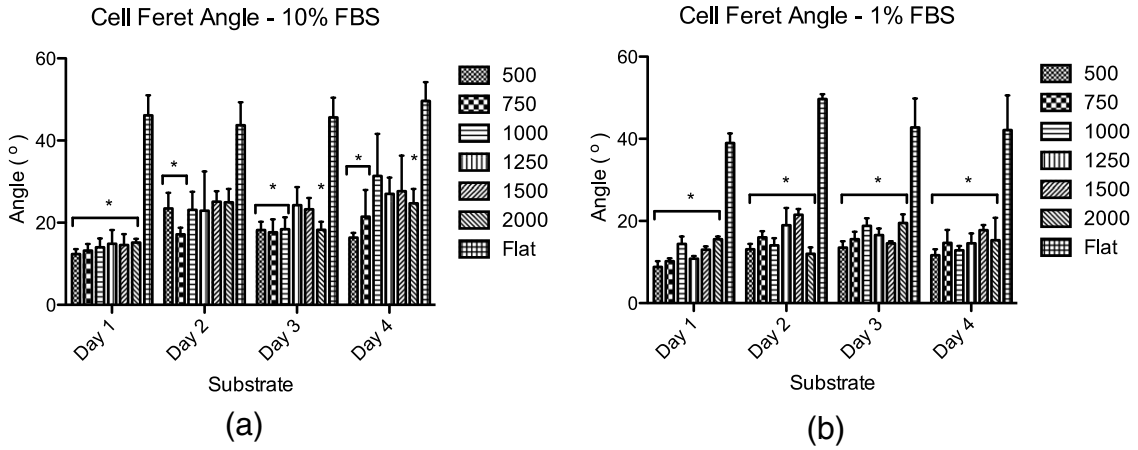

Figure 6. The Feret angle measurements of the cell over a four day period on different substrates. Mean $\pm$SEM, $n = 3$. The asterisks (*) indicate significant differences between the substrates and the flat control ($p < 0.05$). (Mean $\pm$SEM, $n = 3$, >8000 cells measured.)

the 10% FBS condition on day 1 (figure 7(c)), but further concluded that no difference in neurite alignment exists with respect to nanopattern ridge width for the remaining time points.

Based on the assumption that patterned substrates experience statistically similar degrees of alignment, the average neurite angle of all patterned substrates combined was plotted over time. This clearly shows that the alignment angle remains constant under the 1% FBS condition while the 10% FBS condition experiences decreasing alignment. A regular two-way ANOVA analysis comparing daily values of the combined neurite alignment shows that a significant difference between 10% and 1% FBS is established on day 2 and maintained for the remaining days ($p < 0.01$; see figure 7(d)). This can clearly been seen in the angle histograms shown in figure 8, where the neurite angle distribution 1% serum condition remains relatively unchanged over the four day period while the 10% serum condition shows a reduction in alignment.

Overall, the F11 hybridoma cell line adopts a polarized cell morphology when grown on nanopatterned surfaces compared to the control flat surface. The 1% FBS condition shows enhanced neurite outgrowth and consistently induced neurite alignment in response to the underlying nanopattern.

3.4. Cell proliferation

The final cell count shows a general trend, with the 10% serum concentration resulting in a greater cell number over a four day period compared to the 1% serum condition (figure 9). Though not completely statistically significant, this implies that the higher serum concentration leads to increased cell division over this time period.

This is further supported by examining the metabolic activity at days 2 and 4 for both serum conditions on all substrates (figure 10). Although the cell activity remains relatively unchanged for the 1% serum concentration between days 2 and 4, there is a significant increase in metabolic activity for the 10% serum concentration over the same time period.

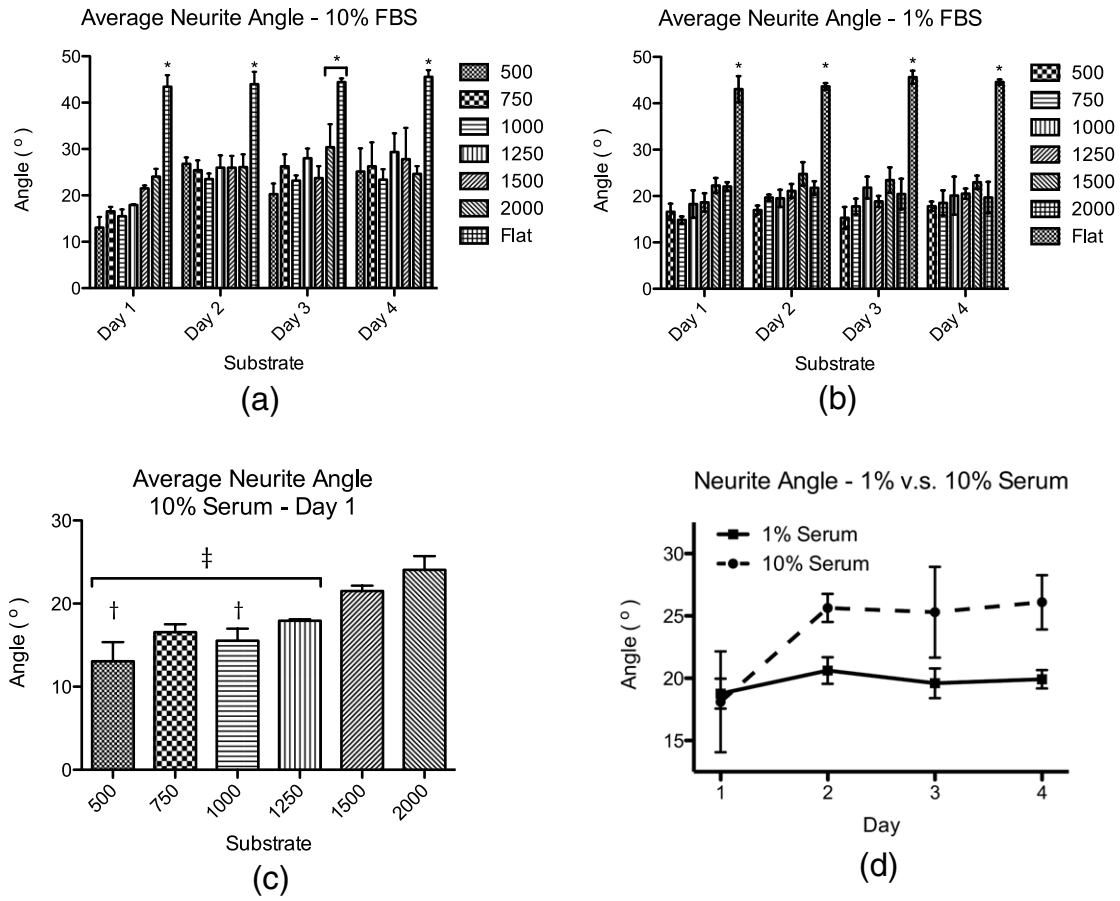

Figure 7. Average neurite alignment angle and SEM for both the (a) 10% FBS and (b) 1% FBS culturing conditions over a four day period on different substrates. (a)–(b) $^{*}p < 0.05$ flat versus all other nanopatterns without the asterisk. Grouping all the patterned substrates together, (c) shows the overall average and SEM of alignment angle for all combined substrates. No difference is observed between conditions on day 1, but a difference is apparent on day 2 ($p < 0.01$) and is maintained for the remaining days. Examining the 10% FBS on day 1 in isolation (d), a one-way ANOVA test reveals that the neurite alignment on the 2000 nm ridge pattern is significantly less compared to the patterns under the line marked with a '‡' and the same on the 1500 nm ridge pattern compared to the patterns marked with a '†'. (Mean ± SEM, $n = 3$, >15 000 neurites analyzed.)

3.5. Focal adhesion analysis

Because of the central role of focal adhesions (FAs) in surface sensing [27], the organization of focal adhesions and actin fibers was visualized by immunostaining. Figures 8 and 9 show focal adhesion formation for the extremes of nanopattern dimensions (flat, 500 nm ridge and 2000 nm ridge patterns) in both 1% FBS and 10% FBS conditions. The cells were immunofluorescently labeled for the focal adhesion components vinculin (green) and actin (red). Vinculin is a protein found in maturing focal adhesions that is involved in the linkage of integrin adhesion molecules to the actin cytoskeleton. The locations where vinculin concentrates or strongly colocalizes with actin (yellow spots) represents where a focal adhesion has formed.

As can be observed from the panels in figures 11 and 12, FAs tend to form at the cell periphery, and in particular along neurites and within growth cones. A qualitative analysis reveals that FAs are more developed in the 10% FBS for both nanopatterns, where they are generally larger and more consolidated. Moreover, improved FA alignment can be observed on the narrower ridge pattern (500 nm) compared to the wider ridge size (2000 nm).

4. Discussion

In general, the response of the F11 cell line to nanotopography was robust under various conditions. Using 1% FBS proved more conducive to measurement and analysis, while the 10% FBS regime provided insight into focal adhesion formation and possible factors affecting guidance.

The present results show that F11 neuronal cells develop a polarized morphology compared to the flat control surface. Both the cell bodies and the neurites align to the nanopattern topography, in particular at a lower FBS concentration (1%).

4.1. Cell morphology

Statistical analysis reveals that the cell body areas and circularity are all roughly equal for all culturing substrates. The 1% serum condition shows an increase in cell area over time, indicating normal cell spreading. The 10% serum

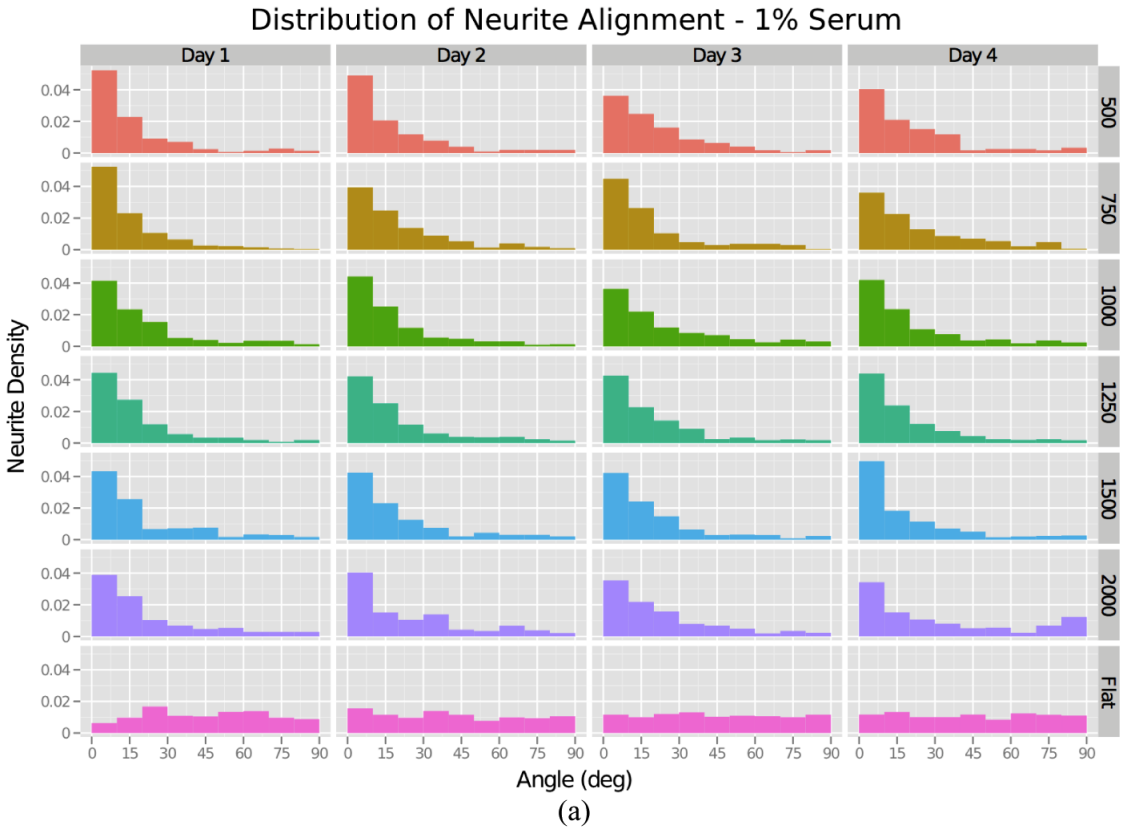

(a)

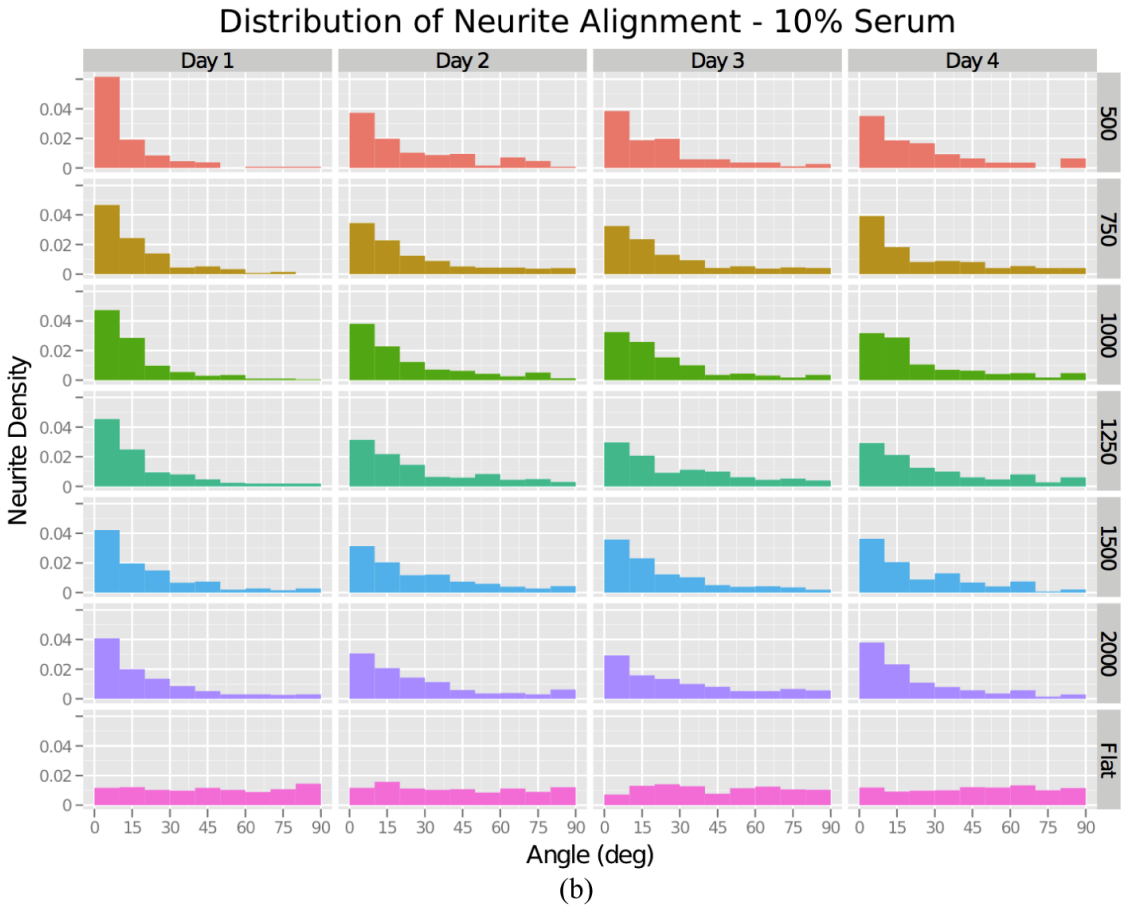

(b)

Figure 8. Histograms of neurite angle distribution for (a) 1% serum and (b) 10% serum, shown over a four day period for all substrates examined (bin size of 10°).

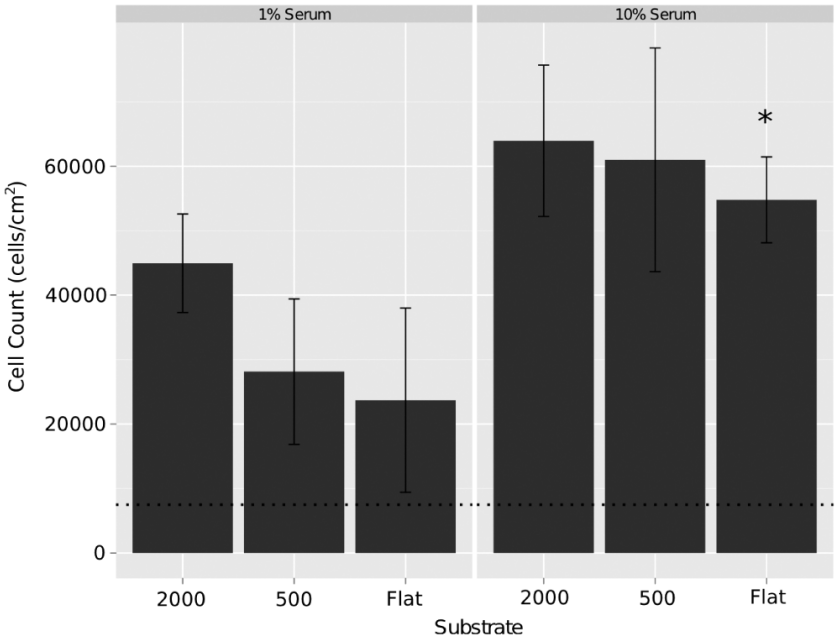

Figure 9. The number of cells present after a four day period. Values are shown for cells on flat substrates and the two extremes of the nanograting patterns (500 and 2000 nm ridge widths). Comparing the 1% serum to the 10% serum, a student T-test found that only the flat substrate was significantly different (*; $p < 0.05$). However, both the 500 and 2000 nm substrates display patterns approaching significance ($p = 0.06$ and $p = 0.089$, respectively). The dotted line represents the initial cell seeding density (mean $\pm$ standard deviation, $n = 3$).

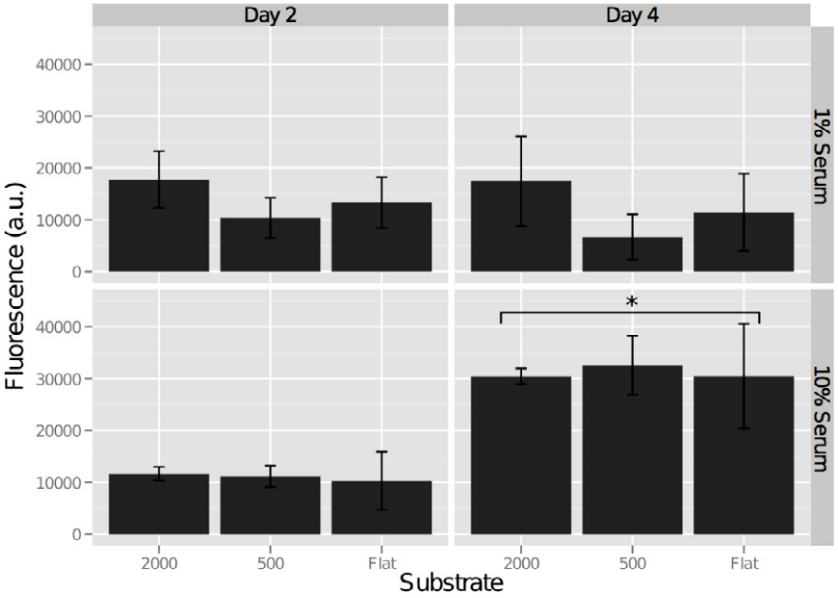

Figure 10. The metabolic activity of F11 cells is shown at days 2 and 4 in 1% serum and 10% serum, on flat substrate and the two extremes of the nanograting patterns: 500 and 2000 nm ridge width (mean $\pm$standard deviation). Per time point, per serum concentration, no significant difference is found between substrates ($p < 0.05$). A significant difference is only found for the 10% serum condition between days 2 and 4 (pair-wise T test, $p < 0.05$).

condition shows a faster increase in cell area that decreases after day 3, likely because of proliferation and reaching a semi-confluent state. This can be attributed to the fact that the serum promotes cells to attach and proliferate, thus the cells grow larger and then divide into smaller cells.

Looking at the neurite length, it seems that the 1% serum regime results in stronger neural differentiation as indicated by longer outgrowth compared to the 10% FBS. In general, the F11 is a suitable model for cell and neurite development and guidance, with extensive outgrowth on nanopatterned substrates that, at times, was in excess of hundreds of micrometers.

4.2. 1% versus 10% serum

There is a degradation in neurite alignment between the 10% and 1% FBS culturing regimes. Comparing the FAs

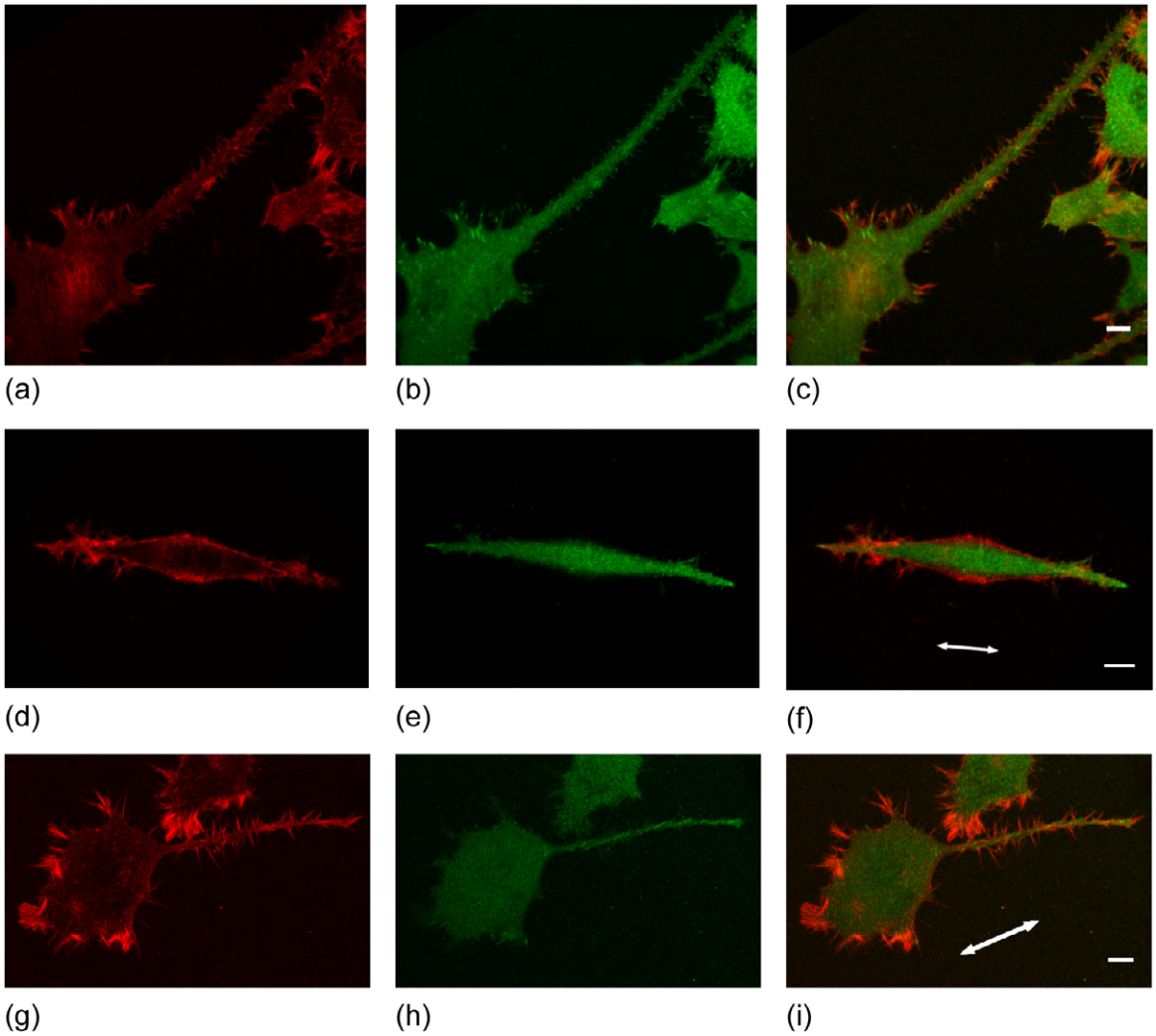

Figure 11. Images of F11 cells grown for one day in 1% FBS on 500 nm ridge patterns (a)–(c), 2000 nm ridge patterns (d)–(f), or flat substrates (g)–(i). The cells were fixed and fluorescently labeled for actin (red; (a), (d), (g)) and vinculin (green; (b), (e), (h)). Merged images of actin and vinculin are also shown to reveal colocalization ((c), (f), (i)). The low intensity vinculin signal seen throughout the cells is cytoplasmic vinculin; focal adhesion-associated vinculin can be distinguished by a greater intensity and actin colocalization. The scale bar indicates 10 mm.

formed in 10% serum to those in 1% serum, they appear larger and more consolidated on both the smallest and the largest nanopatterns examined. The increased serum content may lead to increased deposition of cell-adhesion promoting proteins to the substrate surface [39] or lead to a serum-dependent increase in the production of endogenous extracellular protein [40] to further promote cell adhesion. For this reason, focal adhesion formation could be enhanced. In general, the influence of the underlying nanotopography becomes less significant as cell adhesion is increasingly facilitated [41].

Alternatively, the serum could also modify the focal adhesion dynamics as has been shown in other cell types. For example, Sprouty2 is an intracellular signaling protein present in F11s [36] which is known to modify focal adhesion formation and maturation [42]. Endogenous Sprouty2 (or Spry2) concentration has also been shown to increase with increased medium serum content in mouse cerebellar granule neurons grown *in vitro* [43]. Thus, serum content can directly affect cellular response to underlying topography by affecting FA formation, leading to suboptimal cell path finding [16]. Sprouty2 has even been shown to hinder DRG neurite outgrowth [44, 45], indicating a possible reason for the differences in neurite growth observed in this DRG-derived cell line.

4.3. Neurite guidance in 1% serum and focal adhesion formation

With respect to neurite guidance, the 1% serum conditions revealed that each pattern was able to induce alignment to an equal degree compared to the randomly oriented neurite growth observed on the flat control substrates. Qualitative assessment of focal adhesion formation on nanograting patterns reveals that the 1% serum condition has less consolidated FAs in response to all nanopatterns. This light adherence makes the cells highly responsive to the patterned

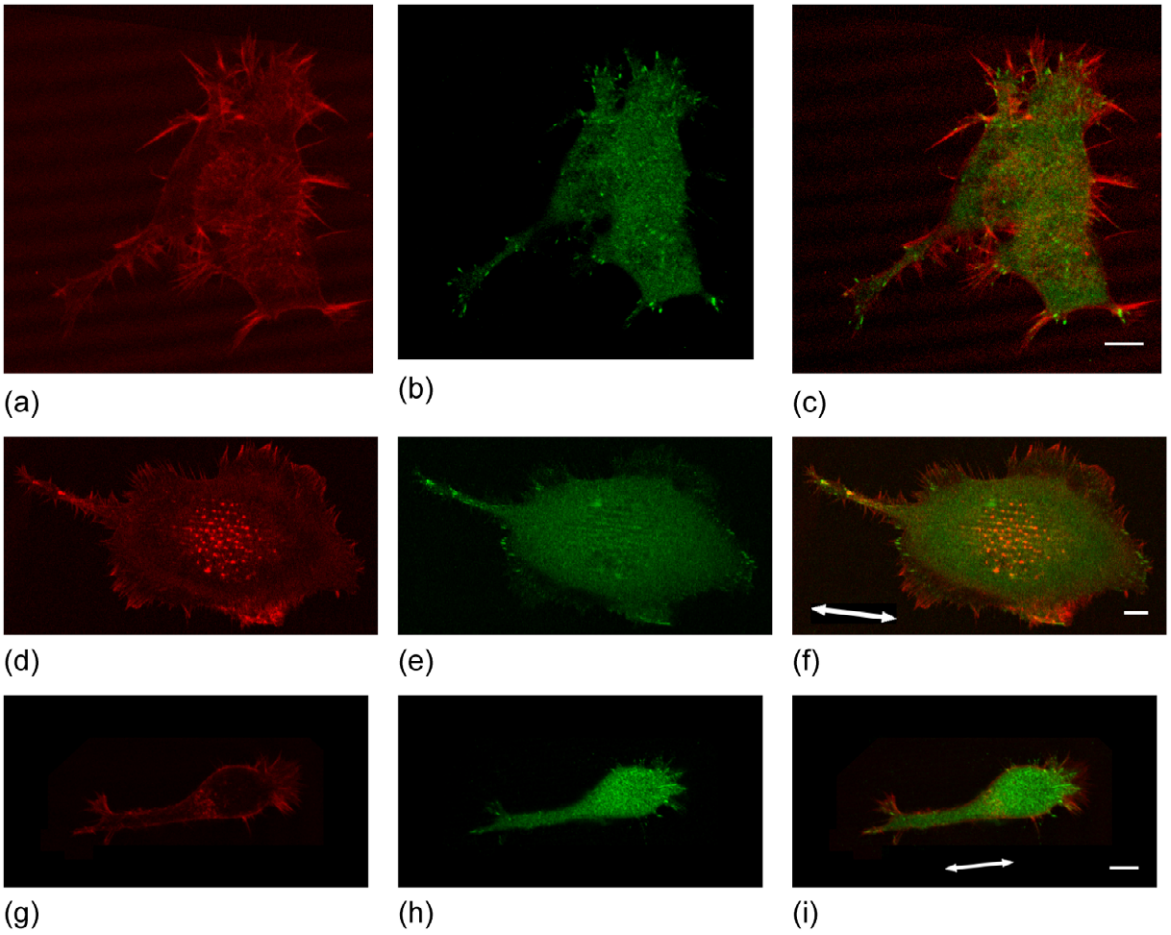

Figure 12. Images of F11 cells grown for 1 day in 10% FBS on 500 nm ridge patterns (a)–(c), 2000 nm ridge patterns (d)–(f), or flat substrates (g)–(i). The cells were fixed and fluorescently labeled for actin (red; (a), (d), (g)) and vinculin (green; (b), (e), (h)). The actin and vinculin are shown separately, then combined in an overlay to reveal colocalization ((c), (f), (i)). The scale bar is 10 mm.

substrate, such that neurite alignment occurs to an equal degree on all patterns.

The ability to achieve equal neurite alignment via differently sized nanotopographical cues opens the possibility of exploring the influence of nanotopography on other aspects of nerve regeneration (speed, selectivity, etc) towards optimized neuro-regenerative scaffolds.

5. Conclusion

The F11 cell line is a highly unique tool in the study of neural regeneration, previously used as an electrically active cell model, as a nociceptor model and for examining regenerative-associated gene (RAG) upregulation. This represents the first time this cell line has been used as a peripheral sensory neuron model for nanotopographical guidance. Under suitable culturing conditions this cell type is capable of extensive neurite outgrowth suitable for axon guidance studies and provides a robust guidance response.

This provides an interesting tool for investigating the influence of nanotopography over adjusting other neurite growth characteristics based on the induction of different focal adhesion sizes (and, thus, different traction forces) without sacrificing neurite guidance. Possibilities include selective guidance of specific neural subtypes, fine tuning Schwann cell scaffold invasion preceding neurite regeneration, or allowing axons to regenerate at equal rates to address issues of reduced functionality which normally occur because some axons naturally regenerate faster than others [46]. Within the scope of tissue scaffold design, the F11 proves to be a promising tool for future development.

Acknowledgments

The authors would like to thank Dr Mirko Klingauf for his insightful discussion and support throughout this study and Dr Lorenzo Moroni, Universtiy of Twente, the Netherlands for his support in finalizing this study. This work was supported partly by the National Science and Research Council of Canada (NSERC), the European Commission through the Projects NANOCARD, NANOII, and MERIDIAN within FP7 and by Regione Toscana through the project ‘Biosensor-based assay for high-throughput quantitative screening of chloride transport’.

References

[1] Meek M F and Coert J H 2002 Clinical use of nerve conduits in peripheral nerve repair: review of the literature *J. Reconstr. Microsurg.* **18** 97–110

[2] Schmidt C E and Leach J B 2003 Neural tissue engineering: strategies for repair and regeneration *Annu. Rev. Biomed. Eng.* **5** 293–347

[3] Belkas J S, Shoichet M S and Midha R 2004 Axonal guidance channels in peripheral nerve regeneration *Oper. Tech. Orthop.* **14** 190–8

[4] Dodla M and Bellamkonda R 2008 Differences between the effect of anisotropic and isotropic laminin and nerve growth factor presenting scaffolds on nerve regeneration across long peripheral nerve gaps *Biomaterials* **29** 33–46

[5] Hu X *et al* 2009 A novel scaffold with longitudinally oriented microchannels promotes peripheral nerve *Tissue Eng.* A **15** 3297–308

[6] Kokai L E, Ghaznavi A M and Marra K G 2010 Incorporation of double-walled microspheres into polymer nerve guides for the sustained delivery of glial cell line-derived neurotrophic factor *Biomaterials* **31** 2313–22

[7] Haastert K, Lipokatic E, Fischer M, Timmer M and Grothe C 2006 Differentially promoted peripheral nerve regeneration by grafted Schwann cells over-expressing different FGF-2 isoforms *Neurobiol. Dis.* **21** 138–53

[8] Guenard V, Kleitman N, Morrissey T K, Bunge R P and Aebischer P 1992 Syngeneic Schwann cells derived from adult nerves seeded in semipermeable guidance channels enhance peripheral nerve regeneration *J. Neurosci.* **12** 3310–20

[9] Mortimer D, Fothergill T, Pujic Z, Richards L J and Goodhill G J 2008 Growth cone chemotaxis *Trends Neurosci.* **31** 90–8

[10] Huber A B, Kolodkin A L, Ginty D D and Cloutier J-F 2003 Signaling at the growth cone: ligand receptor complexes and the control of axon growth and guidance *Annu. Rev. Neurosci.* **26** 509–63

[11] Sundararaghavan H G, Monteiro G A, Firestein B L and Shreiber D I 2009 Neurite growth in 3D collagen gels with gradients of mechanical properties *Biotechnol. Bioeng.* **102** 632–43

[12] Tonazzini I *et al* 2010 Multiscale morphology of organic semiconductor thin films controls the adhesion and viability of human neural cells *Biophys. J.* **98** 2804–12

[13] Craighead H G *et al* 1998 Chemical and topographical surface modification for control of central nervous system cell adhesion *J. Biomed. Microdevice* **1** 49–64

[14] Chiang L-Y *et al* 2011 Laminin-332 coordinates mechanotransduction and growth cone bifurcation in sensory neurons *Nature Neurosci.* **14** 993–1000

[15] Lemmon V, Burden S M, Payne H R, Elmslie G J and Hlavin M L 1992 Neurite growth on different substrates: permissive versus instructive influences and the role of adhesive strength *J Neurosci.* **12** 818–26

[16] Ferrari A, Faraci P, Cecchini M and Beltram F 2010 The effect of alternative neuronal differentiation pathways on PC12 cell adhesion and neurite alignment to nanogratings *Biomaterials* **31** 2565–73

[17] Leipzig N D and Shoichet M S 2009 The effect of substrate stiffness on adult neural stem cell behavior *Biomaterials* **30** 6867–78

[18] Clark P, Connolly P, Curtis A S, Dow J A and Wilkinson C D 1991 Cell guidance by ultrafine topography *in vitro J. Cell Sci.* **99** 73–7

[19] Johansson F, Carlberg P, Danielsen N and L 2006 Axonal outgrowth on nano-imprinted patterns *Biomaterials* **27** 1251–8

[20] Chew S Y, Mi R, Hoke A and Leong K W 2007 Aligned protein–polymer composite fibers enhance nerve regeneration: a potential tissue-engineering platform *Adv. Funct. Mater.* **17** 1288–96

[21] Kim Y-T, Haftel V K, Kumar S and Bellamkonda R V 2008 The role of aligned polymer fiber-based constructs in the bridging of long peripheral nerve gaps *Biomaterials* **29** 3117–27

[22] Fozdar D Y, Lee J Y, Schmidt C E and Chen S 2010 Hippocampal neurons respond uniquely to topographies of various sizes and shapes *Biofabrication* **2** 035005

[23] Rajnicek A M, Britland S and McCaig C D 1997 Contact guidance of CNS neurites on grooved quartz: influence of groove dimensions, neuronal age and cell type *J. Cell Sci.* **110** 2905–13

[24] Ferrari A *et al* 2011 Nanotopographic control of neuronal polarity *Nano Lett.* **11** 505–11

[25] Franco D *et al* 2011 Control of initial endothelial spreading by topographic activation of focal adhesion kinase *Soft Matter* **7** 7313–24

[26] Geiger B, Spatz J P and Bershadsky A D 2009 Environmental sensing through focal adhesions *Nature Rev. Mol. Cell Biol.* **10** 21–33

[27] Scales T M and Parsons M 2011 Spatial and temporal regulation of integrin signalling during cell migration *Curr. Opin. Cell Biol.* **23** 562–8

[28] Cecchini M, Bumma G, Serresi M and Beltram F 2007 PC12 differentiation on biopolymer nanostructures *Nanotechnology* **18** 1–7

[29] Francel P C, Harris K, Smith M, Fishman M C, Dawson G and Miller R J 1987 Neurochemical characteristics of a novel dorsal root ganglion X neuroblastoma hyrbrid cell line, F-11 *J. Neurochem.* **48** 1624–31

[30] Boland L M and Dingledine R 1990 Expression of sensory neuron antigens by a dorsal root ganglion cell line, F-11 *Dev. Brain Res.* **51** 259–66

[31] Jahnel R, Bender O, Munter L M, Dreger M, Gillen C and Hucho F 2003 Dual expression of mouse and rat VRL-1 in the dorsal root ganglion derived cell line F-11 and biochemical analysis of VRL-1 after heterologous expression *Eur. J. Biochem.* **270** 4264–71

[32] Vetter I and Lewis R J 2009 Characterization of endogenous calcium responses in neuronal cell lines *Biochem. Pharmacol.* **79** 908–20

[33] Bender F L P *et al* 2005 The temperature-sensitive Ion channel TRPV2 is endogenously expressed and functional in the primary sensory cell line F-11 *Cell Physiol. Biochem.* **15** 183–94

[34] McIlvain H B *et al* 2006 Pituitary adenylate cyclase-activating peptide (PACAP) induces differentiation in the neuronal F11 cell line through a PKA-dependent pathway *Brain Res.* **1077** 16–23

[35] Borgesius N Z *et al* 2011 β CaMKII plays a nonenzymatic role in hippocampal synaptic plasticity and learning by targeting α CaMKII to synapses *J. Neurosci.* **31** 10141–8

[36] MacGillavry H D, Cornelis J, van der Kallen L R, Sassen M M, Verhaagen J, Smit A B and van Kesteren R E 2011 Genome-wide gene expression and promoter binding analysis identifies NFIL3 as a repressor of C/EBP target genes in neuronal outgrowth *Mol. Cell. Neurosci.* **46** 460–8

[37] Holtzman D M *et al* 1995 Low density lipoprotein receptor-related protein mediates apolipoprotein E-dependent neurite outgrowth in a central nervous system-derived neuronal cell line *Proc. Natl. Acad. Sci.* **92** 9480–4

[38] Nah S Y, Unteutsch A, Bunzow J R, Cook S P, Beacham D W and Grandy D K 1997 m and d opioids but not k opioid inhibit voltage-activated Ba2+ currents in neuronal F-11 cell *Brain Res.* **766** 66–71

[39] Hayman E G and Pierschbacher M D 1985 Vitronectin—a major cell attachment-promoting protein in fetal bovine serum sera and serum proteins isolation of vitronectin antisera and immunoassays *Exp. Cell Res.* **160** 245–58

[40] Johnson P R, Black J L, Carlin S, Ge Q and Underwood P A 2000 The production of extracellular matrix proteins by human passively sensitized airway smooth-muscle cells in culture: the effect of

beclomethasone *Am. J. Respir. Crit. Care Med.* **162** 2145–51
[41] Dalby M J, Hart A and Yarwood S J 2008 The effect of the RACK1 signalling protein on the regulation of cell adhesion and cell contact guidance on nanometric grooves *Biomaterials* **29** 282–9
[42] Lee C-C *et al* 2004 Overexpression of sprouty 2 inhibits HGF/SF-mediated cell growth, invasion, migration, and cytokinesis *Oncogene* **23** 5193–202
[43] Gross I *et al* 2007 Sprouty2 inhibits BDNF-induced signaling and modulates neuronal differentiation and survival *Cell Death Differ.* **14** 1802–12
[44] Strickland I T, Richards L, Holmes F E, Wynick D, Uney J B and Wong L-F 2011 Axotomy-induced miR-21 promotes axon growth in adult dorsal root ganglion neurons *PloS One* **6** e23423
[45] Hausott B *et al* 2009 Sprouty2 downregulation promotes axon growth by adult sensory neurons *Mol. Cell Neurosci.* **42** 328–40
[46] Negredo P, Castro J, Lago N, Navarro X and Avendan O C 2004 Differential growth of axons from sensory and motor neurons through a regenerative electrode: a stereological, retrograde tracer, and functional study in the rat *Neuroscience* **128** 605–15